(12)

ARL-TR-92-12

Copy No. 69

Bottom Penetration at Shallow Grazing Angles II

Final Report under Contract N00039-91-C-0082,
TD No. 01A1006, Bottom Penetration at Shallow Grazing Angles II

Frank A. Boyle
Nicholas P. Chotiros

Applied Research Laboratories
The University of Texas at Austin
P. O. Box 8029 Austin, TX 78713-8029

19 June 1992

Final Report

31 December 1990 - 31 December 1991

Approved for public release; distribution is unlimited.

Prepared for:
Naval Research Laboratory
Stennis Space Center, MS 39529-5004

Monitored by:
Space and Naval Warfare Systems Command
Department of the Navy
Washington, D.C. 20363-5100

REPORT DOCUMENTATION PAGE

Form Approved
OMB No. 0704-0188

1. AGENCY USE ONLY (Leave blank)	2. REPORT DATE	3. REPORT TYPE AND DATES COVERED
	19 Jun 92	final, 31 Dec 90 - 31 Dec 91

4. TITLE AND SUBTITLE
Bottom Penetration at Shallow Grazing Angles II
Final Report under Contract N00039-91-C-0082, TD No. 01A1006, Bottom Penetration at Shallow Grazing Angles II

5. FUNDING NUMBERS
N00039-91-C-0082,
TD No. 01A1006

6. AUTHOR(S)
Boyle, Frank A. Chotiros, Nicholas P.

7. PERFORMING ORGANIZATION NAMES(S) AND ADDRESS(ES)
Applied Research Laboratories
The University of Texas at Austin
P.O. Box 8029
Austin, Texas 78713-8029

8. PERFORMING ORGANIZATION REPORT NUMBER
ARL-TR-92-12

9. SPONSORING/MONITORING AGENCY NAME(S) AND ADDRESS(ES)
Naval Research Laboratory
Stennis Space Center, Mississippi 39529-5004

10. SPONSORING/MONITORING AGENCY REPORT NUMBER

11. SUPPLEMENTARY NOTES

12a. DISTRIBUTION/AVAILABILITY STATEMENT
Approved for public release; distribution is unlimited.

12b. DISTRIBUTION CODE

13. ABSTRACT (Maximum 200 words)

A study was made of acoustic propagation through sandy sediments. It was done in two parts. First an acoustic model for penetration based on the Biot model was considered. The model was used to predict phase velocities, attenuations, reflection coefficients, and pressure amplitudes in the sediment. Second, a preliminary model for acoustic backscatter from a distribution of gas bubbles was developed. The model involves a combination of existing theories for backscattering strengths from individual bubbles with a hypothetical bubble size distribution function which is related to the sediment grain size distribution.

14. SUBJECT TERMS
backscatter, Biot, bubble, bubble size distribution, gassy sediment, porous medium, sediment

15. NUMBER OF PAGES
43

16. PRICE CODE

17. SECURITY CLASSIFICATION OF REPORT	18. SECURITY CLASSIFICATION OF THIS PAGE	19. SECURITY CLASSIFICATION OF ABSTRACT	20. LIMITATION OF ABSTRACT
UNCLASSIFIED	UNCLASSIFIED	UNCLASSIFIED	SAR

This page intentionally left blank.

TABLE OF CONTENTS

		Page
LIST OF FIGURES		v
PREFACE		vii
EXECUTIVE SUMMARY		ix
1.	INTRODUCTION	1
2.	ACOUSTIC PROPAGATION MODELING	3
	2.1 MODEL DESCRIPTION	3
	2.2 RESULTS	5
3.	SCATTERING	15
	3.1 OVERVIEW	15
	3.2 STATISTICAL STUDY	15
	3.3 PRELIMINARY MODEL	18
	3.3.1 Bubble Size Distribution	18
	3.3.2 Scattering Integral	23
	3.3.3 Comparison with Experiment	23
4.	CONCLUSION	27
APPENDIX -	A COMPARISON OF THE BIOT EQUATIONS AS GIVEN BY STERN TO THOSE ORIGINALLY PUBLISHED BY BIOT	29

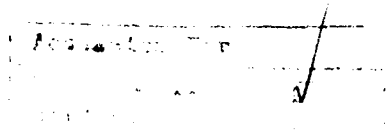

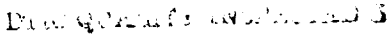

A-1

This page intentionally left blank.

LIST OF FIGURES

Figure		Page
2.1	Biot Predictions of Wavespeeds, 60 kHz	6
2.2	Biot Predictions of Reflection Coefficient versus Frequency and Gas Fraction	7
2.3	Biot Model Contour Comparison: log(gas fraction) = -7	8
2.4	Biot Model Contour Comparison: log(gas fraction) = -6	9
2.5	Biot Model Contour Comparison: log(gas fraction) = -5	10
2.6	Biot Model Contour Comparison: log(gas fraction) = -4	11
2.7	Biot Model Contour Comparison: log(gas fraction) = -3	12
2.8	Biot Predictions of Pressure versus Depth and Grazing Angle at a Frequency of 120 kHz	13
3.1	Experimental Measurements of Bottom Backscattering Strength as a Function of Grain Size at a Grazing Angle of 10° from All Published Sources	16
3.2	Experimental Measurements of Bottom Backscattering Strength as a Function of Grain Size at a Grazing Angle of 10°, Groups 1 and 2	17
3.3	Close Packed Sediment Grains	19
3.4	A Comparison of Experimental Data with Backscattering Strengths Predicted by Eq. (3.15)	24

This page intentionally left blank.

PREFACE

This final report covers the work that Applied Research Laboratories was tasked to perform under Contract N00039-91-C-0082, TD No. 01A1006, entitled Bottom Penetration at Shallow Grazing Angles II.

This page intentionally left blank.

EXECUTIVE SUMMARY

This work was conducted under Task Description 01A1006, titled Bottom Penetration at Shallow Grazing Angles II. The objective is a new theory of acoustic penetration of sandy sediments that will address the shortcomings of current models, and lead to improved bottom backscattering models.

Recent studies of experimental data suggest that current models for acoustic penetration and backscatter might be improved in two ways. First, by incorporating the Biot theory, a more appropriate model for refraction of acoustic waves into the bottom may be obtainable. Second, the inclusion of the effects of trapped gas bubbles might improve predictions of backscattering strength of sediments. The first of the above modifications was suggested by the results of experiments at sea by Chotiros and in a laboratory tank by Boyle and Chotiros. In these experiments a slow acoustic wave that appears consistent with the Biot theory was observed. This slow wave affects the bottom penetration problem significantly, particularly at shallow grazing angles where previous theories predict no refractive penetration. The second modification was suggested by Chotiros and Boyle in a compilation of previous experimental data. Much of the data exhibited a broad maximum in the backscattering strength spectrum that appeared consistent with resonances involving bubbles of radii comparable to the mean pore size.

A model for acoustic penetration based on the Biot theory was modified to allow for a change in fluid compressibiltity due to trapped gas. It is noteworthy that, except for high gas fractions, a significant amount of acoustic energy is predicted to penetrate the sediment, even when the grazing angle is very shallow. Other interesting predictions of ihis model were a minimum in the reflection coefficient when the gas fraction is between 10^{-5} and 10^{-4} and a spatial interference pattern between Biot slow and fast wave contributions to the total sediment pressure. The interference pattern has not yet been observed experimentally, possibly because of scattering.

A preliminary backscatter model was developed that accounts for trapped bubble resonances. The results of this model were compared to

experimental results. At gas fractions between $4x10^{-5}$ and $5x10^{-6}$, this preliminary model predicts backscattering strengths that are generally consistent with extant experimental data.

In conclusion, the analysis shows that inclusion of the Biot theory affects the bottom penetration significantly. Also, experiments suggest that sediment gas bubbles may account for a considerable portion of sediment acoustic backscatter. In the next task, the Biot model and the sediment bubble scattering model will be combined.

1. INTRODUCTION

The applicability of the Biot theory to acoustic propagation in sandy sediments was suggested by recent experimental results at sea[1,2] and in a laboratory tank.[3] These experiments detected the existence of a slow compressional acoustic wave similar to that predicted by the Biot theory. The influence of this particular wave may have significant impact on bottom penetration, particularly at shallow grazing angles. In this regime the slow wave's speed allows it to penetrate while the fast wave reflects totally back up into the water column. The slow wave might therefore contribute significantly to shallow grazing angle volume backscatter from sediments, and a theory that includes this wave is essential.

The influence of gas on the backscattering strength of sandy sediments is suggested by a compilation of backscatter data taken by Chotiros.[4] The backscattering strength spectrum at several sites exhibits a broad maximum that appears consistent with a probable mean bubble radius.

The mechanism for acoustic interaction with the ocean bottom will be treated in two parts. First, a model derived from the Biot theory[5,6] for acoustic penetration into sandy sediments will be discussed. Second, a model for acoustic backscatter from entrapped gas will be considered. Combining the two will lead to a model of bottom backscatter from gas bubbles.

In this report, the two models are developed separately. Further development and integration will be accomplished under follow-on tasks.

This page intentionally left blank.

2. ACOUSTIC PROPAGATION MODELING

2.1 MODEL DESCRIPTION

The theoretical work for this project begins with a model for reflection and transmission devised by Stern and Bedford.[7] A comparison of the Biot's displacement equations as given by Stern with those originally published by Biot is given in Appendix A. This particular model is based on the Biot theory, which predicts the existence of two compressional waves. The model was selected because previous experimental work[8-10] suggests the possible existence of two separate compressional waves. Various modifications were made to Stern's model to enable calculation of reflection and transmission coefficients, and to model the effect of gas bubbles in the pore fluid.

The existence of gas in the sediment was modeled by varying the complex compressibility and density of the fluid phase appropriately. The gas contribution to these parameters was obtained from a theory developed by Hawkins and Bedford[11] involving reflection coefficients from bubbles. The theory includes resonance phenomena involving a distribution of bubble radii. It is an extension of previous work involving propagation through uniform bubbles. There is no allowance for coupling between individual bubbles. A log normal bubble size distribution is assumed and the mean and variance of bubble size are specified. For this purpose an assumption was made that bubbles in the sediment have radii comparable to the pore radius.

The model predicts phase velocities, attenuations, reflection coefficients, and pressure amplitudes in the sediment as functions of depth, grazing angle, gas content, and frequency. The input parameters are listed in Table 2.1. They were chosen to model sandy sediment and are generally the same parameter values used by Stern and Bedford[12] with two exceptions. The exceptions were made based on acoustic analysis results of bottom penetration into sand from the Kings Bay experiment, the Panama City experiment, and most recently from an experiment in the Applied Research Laboratories, The University of Texas at Austin (ARL:UT) sand tank.

TABLE 2.1
BIOT MODEL INPUT PARAMETERS

Fluid Density	1000	kg/m^3
Fluid Bulk Modulus	2.0×10^9	Pa
Porosity	0.47	
Grain Density	2650	kg/m^3
Pore Size	1.0×10^{-5}	m
Viscosity	1.0×10^{-3}	kg/m-s
Permeability	1.0×10^{-10}	m^2
Grain Bulk Modulus	0.9×10^{10}	Pa
Frame Shear Modulus	2.61×10^7	Pa
Shear Logarithmic Decrement	0.15	
Frame Bulk Modulus	4.36×10^9	Pa
Bulk Logarithmic Decrement	0.15	
Virtual Mass Parameter	1.25	
Gas Bulk Modulus	2.48×10^5	Pa
Average Bubble Radius	1.0×10^{-5}	m
Standard Deviation in Bubble Radius	5.0×10^{-6}	m

One exception is the grain bulk modulus. No direct experimental measurements of this quantity could be found by the authors. The original grain bulk modulus used by Stern was chosen to be that of pure quartz crystals. Since sands in general contain imperfections and impurities it is reasonable that the actual grain bulk modulus may differ significantly from this value. The acoustic analysis results mentioned above suggest a value less than Stern's by a factor of four. Current work on a direct measurement of this parameter[13] appears to support these acoustic analysis results. The other exception is the frame bulk modulus. The acoustic analysis results suggested a value ten times greater than Stern's.

The gas bubble size in this analysis was assumed to reflect that of the grains of sand in the sediment. The bubble mean diameter was set equal to the pore size. Further work on an accurate estimation of the bubble population distribution is in progress. Some of this work is described in Section 3.2.

It is noteworthy that some of the Biot input parameter values are still somewhat uncertain. Other parameters, such as the virtual mass parameter, are also difficult to determine. The parameters tabulated in Table 2.1 are the best that can be determined at the present time.

2.2 RESULTS

The model was used to predict acoustic wave speeds in the sediment, the reflection coefficient, and penetration loss. The results are shown in Figs. 2.1 - 2.8.

Figure 2.1 is a plot of the phase velocities of the Biot fast, slow, and shear waves as functions of gas content at 60 kHz. Similar plots were computed at 30 and 120 kHz and they appear virtually identical. The slow wavespeed appears to be quite sensitive to gas content when the gas fraction is greater than 10^{-5}.

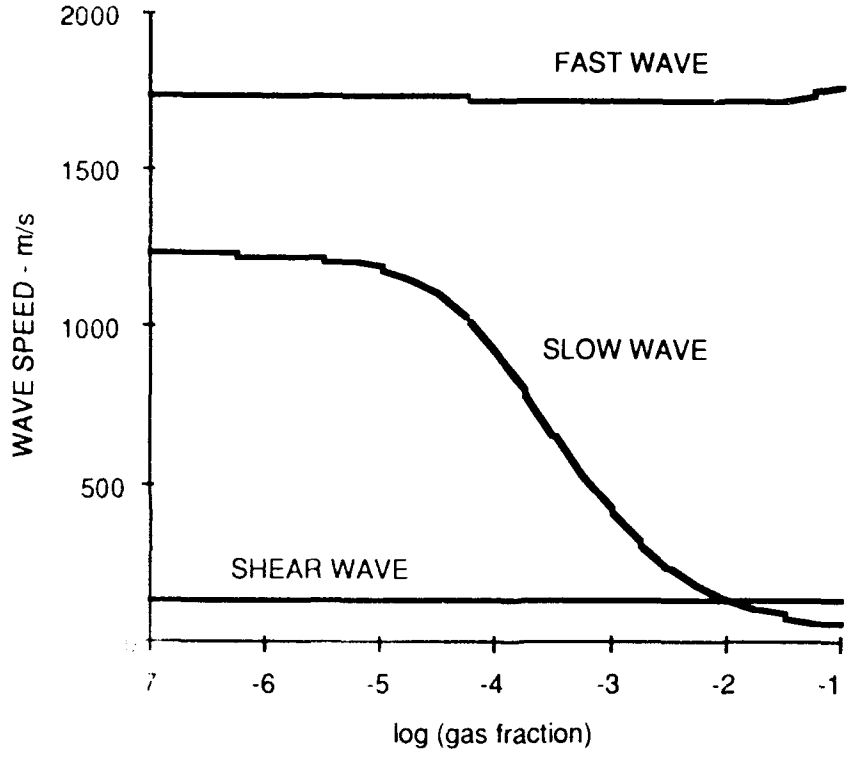

FIGURE 2.1
BIOT PREDICTIONS OF WAVESPEEDS, 60 kHz

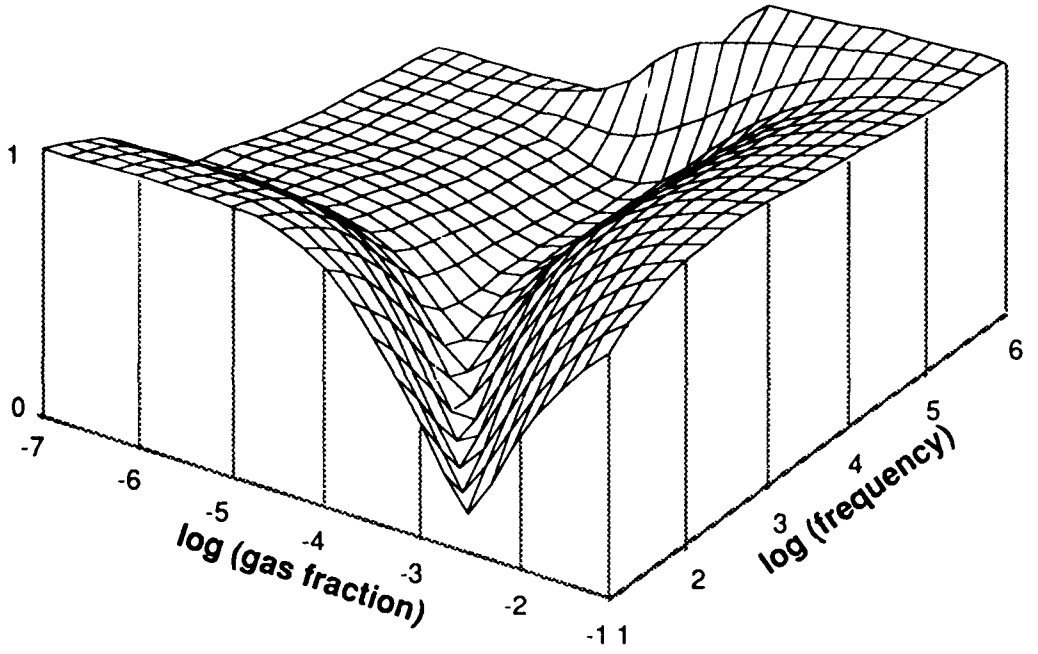

FIGURE 2.2
BIOT PREDICTIONS OF REFLECTION COEFFICIENT versus FREQUENCY AND GAS FRACTION

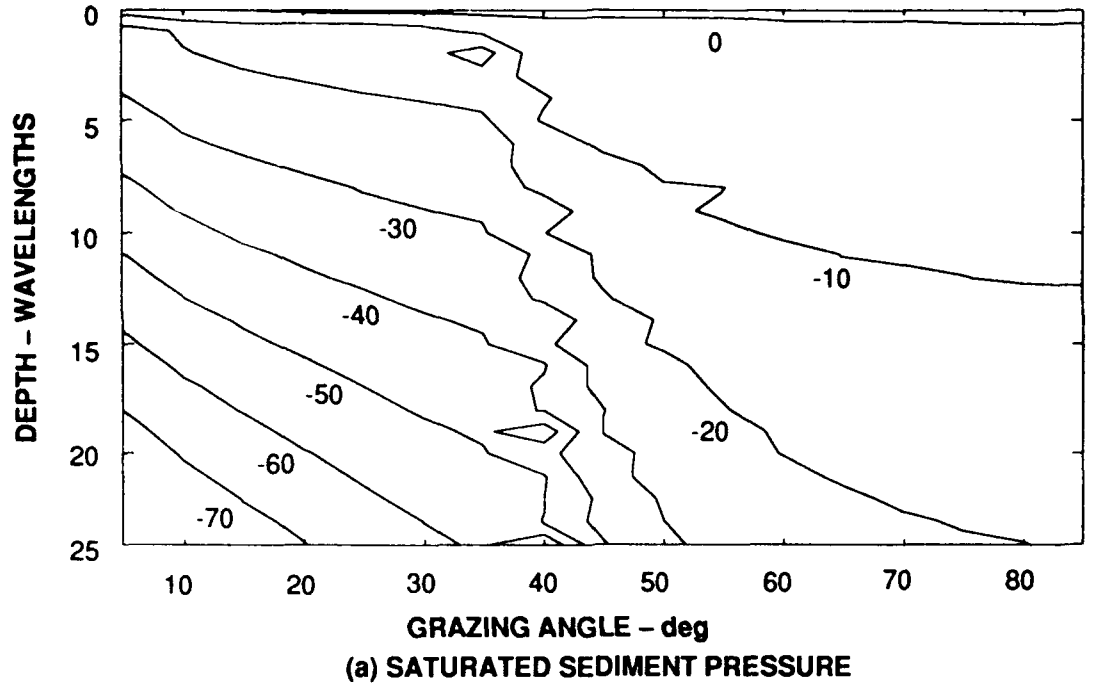

(a) SATURATED SEDIMENT PRESSURE

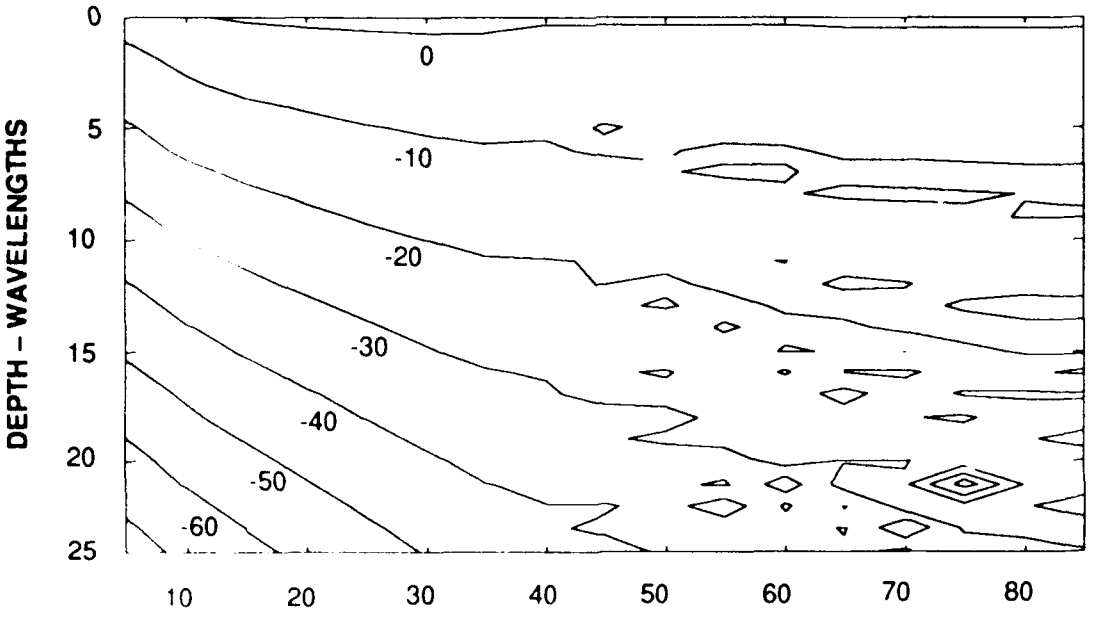

(b) PORE PRESSURE

FIGURE 2.3
BIOT MODEL CONTOUR COMPARISON
(dB re Surface Pressure)
60 kHz
log (gas fraction) = -7

ARL UT
AS-92-158
FAB - DS
7 - 1 - 92

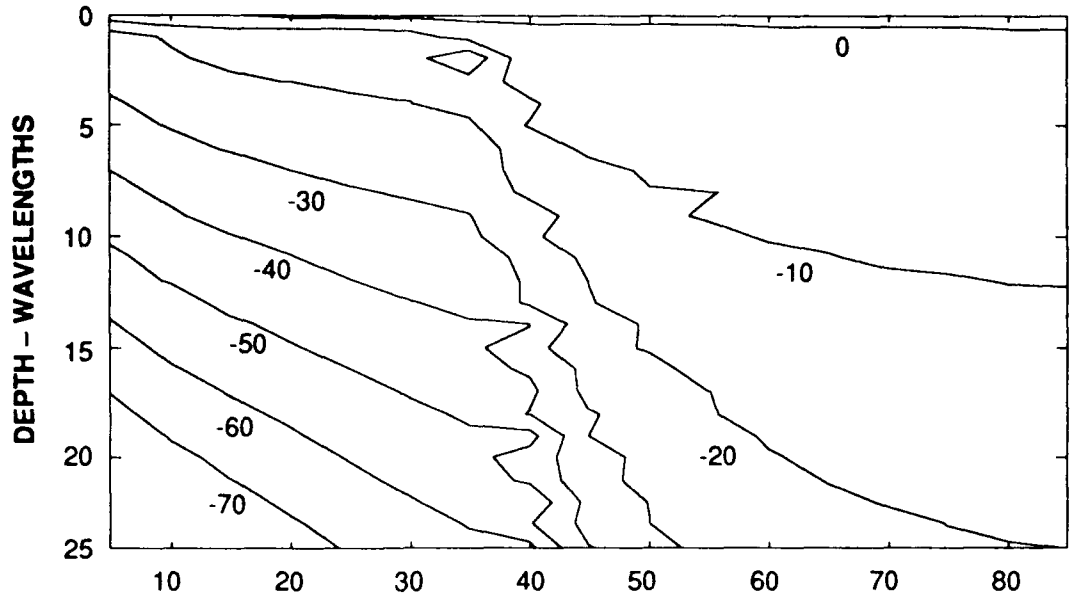

(a) SATURATED SEDIMENT PRESSURE

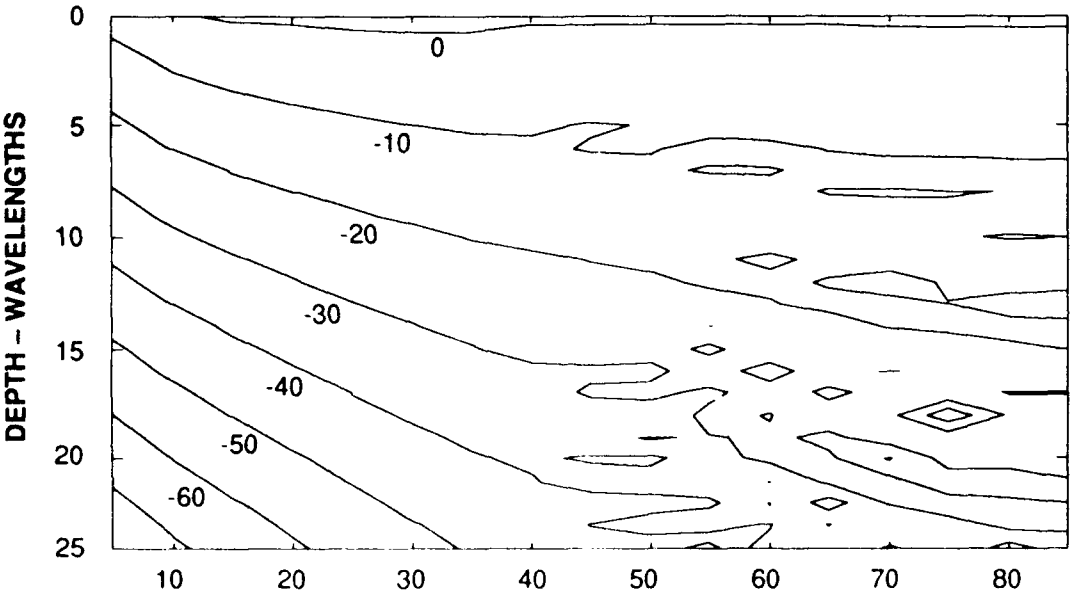

(b) PORE PRESSURE

FIGURE 2.4
BIOT MODEL CONTOUR COMPARISON
(dB re Surface Pressure)
60 kHz
log (gas fraction) = -6

ARL:UT
AS-92-159
FAB - DS
7 - 1 - 92

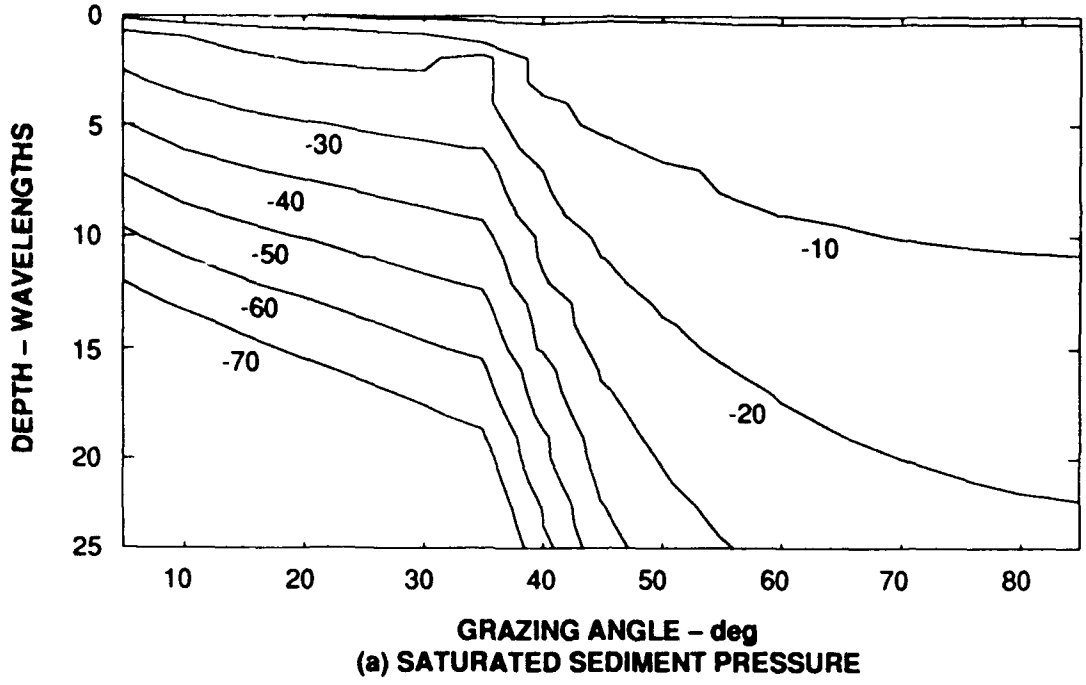

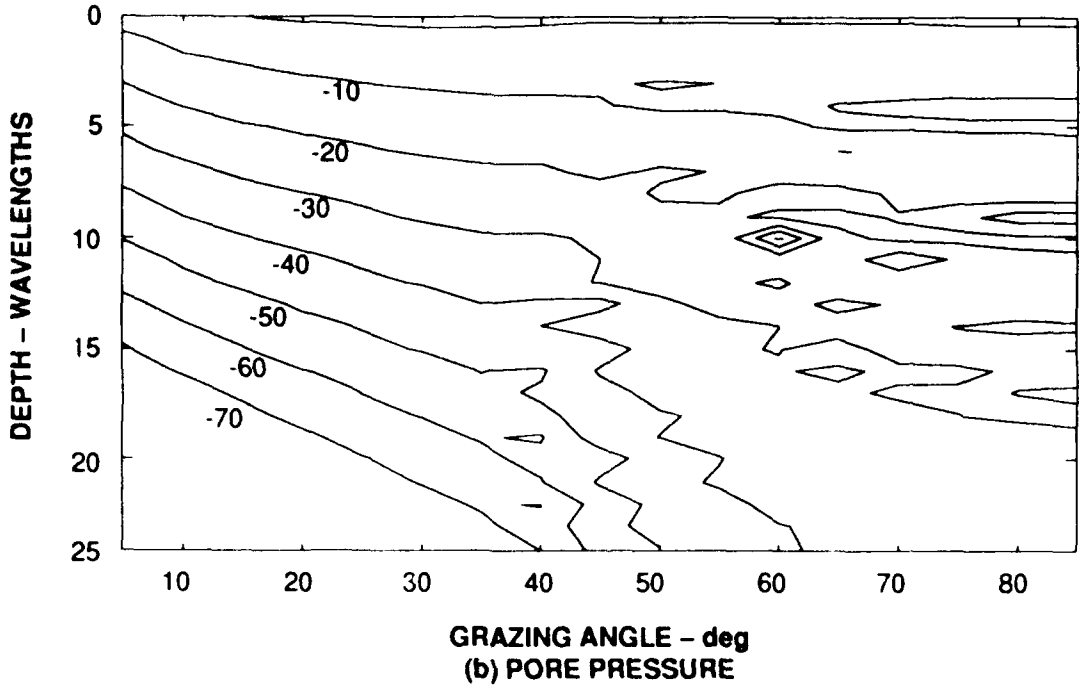

FIGURE 2.5
BIOT MODEL CONTOUR COMPARISON
(dB re Surface Pressure)
60 kHz
log (gas fraction) = -5

ARL:UT
AS-92-160
FAB - DS
7 - 1 - 92

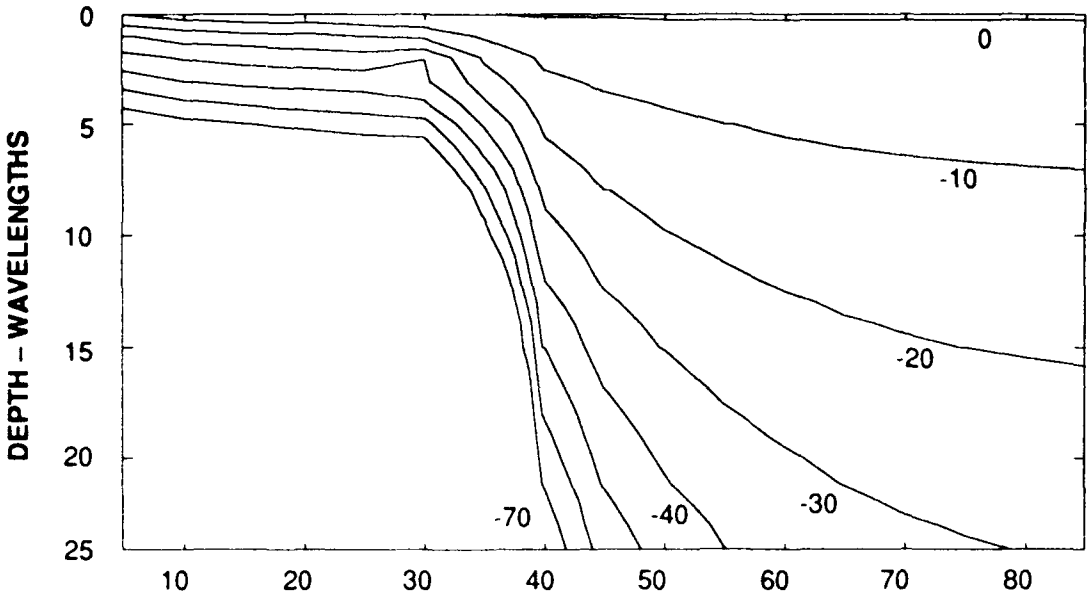

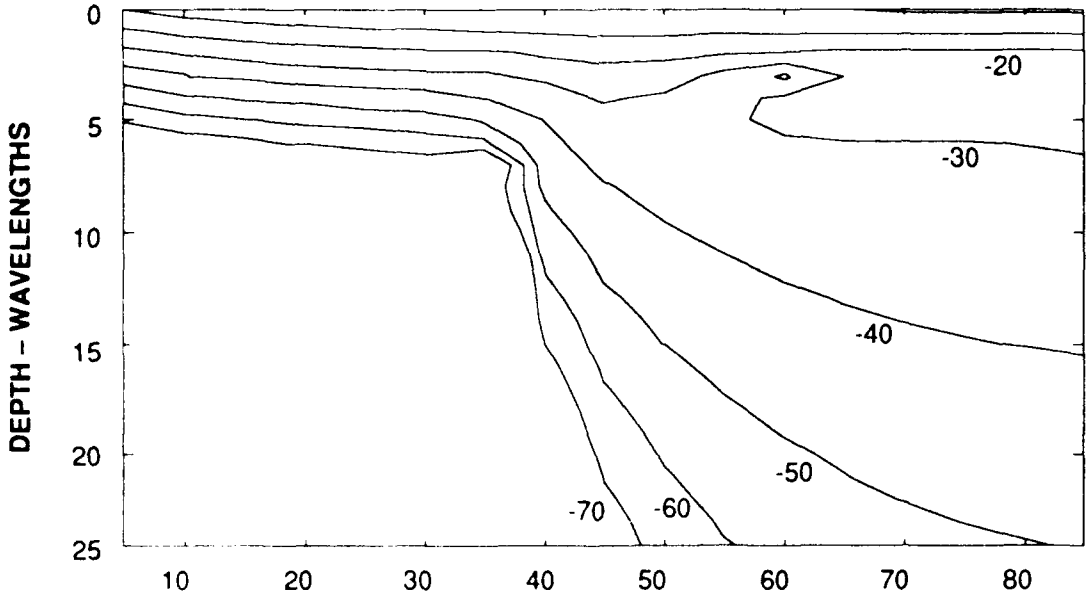

FIGURE 2.6
BIOT MODEL CONTOUR COMPARISON
(dB re Surface Pressure)
60 kHz
log (gas fraction) = -4

ARL:UT
AS-92-161
FAB - DS
7 - 1 - 92

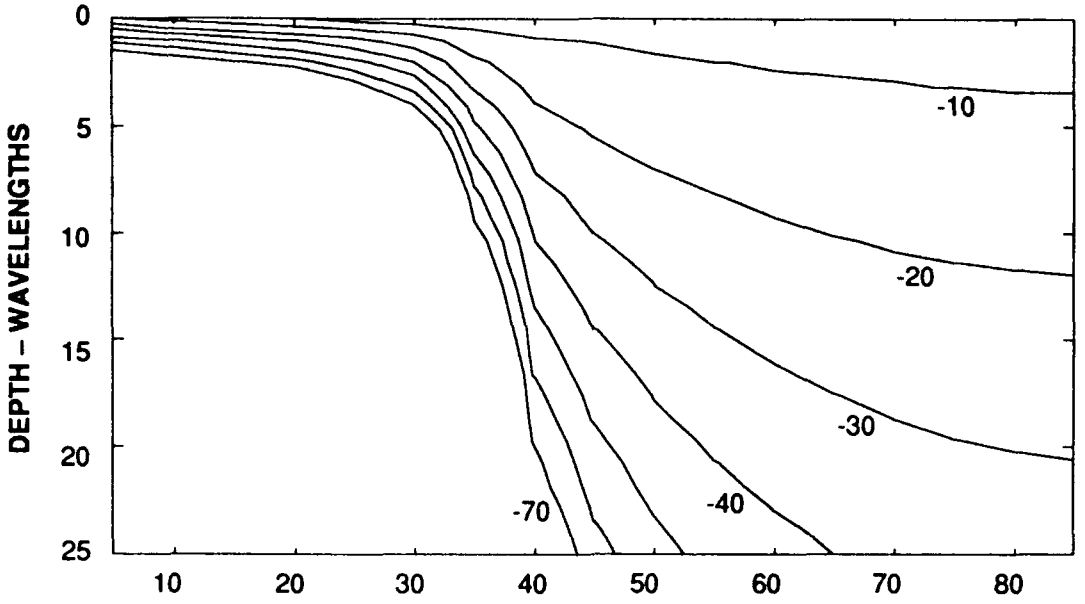

GRAZING ANGLE – deg
(a) SATURATED SEDIMENT PRESSURE

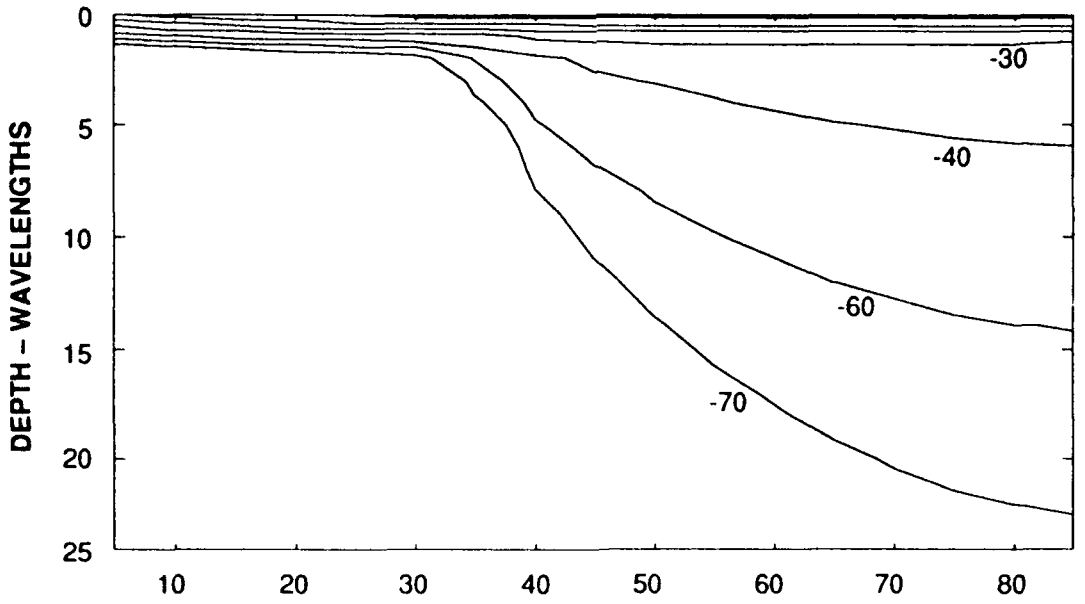

GRAZING ANGLE – deg
(b) PORE PRESSURE

FIGURE 2.7
BIOT MODEL CONTOUR COMPARISON
(dB re Surface Pressure)
60 kHz
log (gas fraction) = -3

ARL:UT
AS-92-162
FAB - DS
7 - 1 - 92

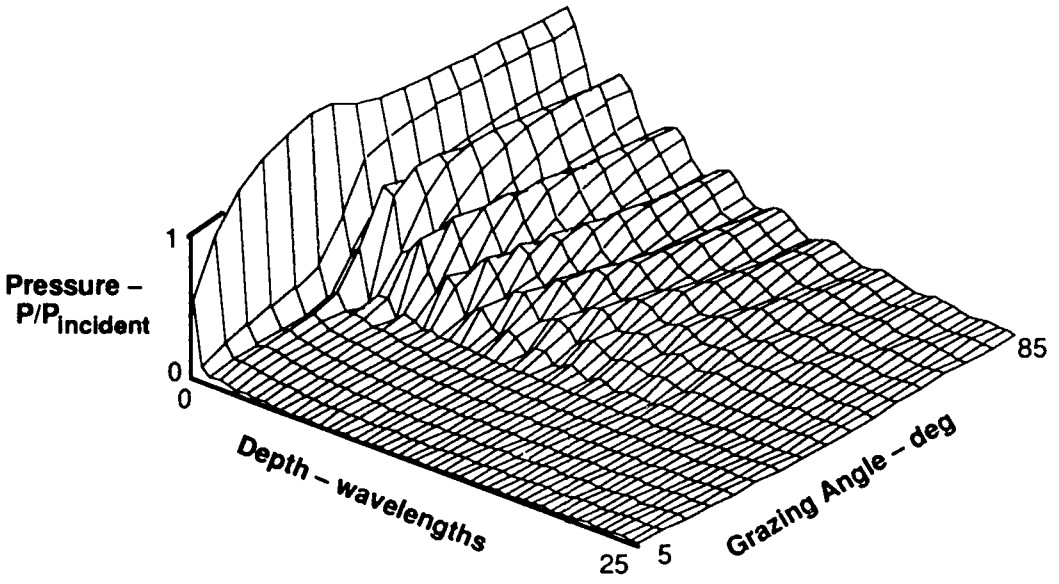

FIGURE 2.8
BIOT PREDICTIONS OF PRESSURE versus DEPTH AND GRAZING ANGLE AT A FREQUENCY OF 120 kHz

Figure 2.2 is a three-dimensional mesh plot of the reflection coefficient as a function of gas content and frequency at a grazing angle of 15°. Noteworthy is a broad minimum in the reflection coefficient at a gas fraction of between 10^{-5} and 10^{-4} in the frequency band of interest between 30 and 120 kHz.

Figures 2.3 - 2.7 are contour plots of the pore pressure and saturated sediment pressure amplitudes as functions of depth and grazing angle at a frequency of 60 kHz and gas fractions of 10^{-7} to 10^{-3}. Such contour plots were also made at 30 and 120 kHz. These looked almost identical to those taken at 60 kHz. On a dimensionless depth scale measured in wavelengths at the speed of sound in water, there is apparently very little frequency dependence in the pressure amplitude. At large gas fractions, greater than 10^{-3}, there is very little pressure transmitted at shallow grazing angles. Otherwise significant penetration is predicted at all angles.

Figure 2.8 is a three-dimensional mesh plot of the saturated sediment pressure. It is interesting that a standing interference pattern is predicted, caused by the interference of the Biot fast and slow waves. So far this interference pattern has not been detected experimentally, possibly because of scattering.

The present model can only accommodate plane waves in the fluid above. Work is in progress to allow the accommodation of spherical or cylindrical waves. Work is also in progress to allow computation of transmission coefficients for each of the Biot waves.

Of ultimate interest is the volume backscatter intensity from gassy sediments. Once the problem of transmission into the sediment has been solved, current work on acoustic backscatter from bubble distributions will be used to arrive at a model for backscatter from bubble distributions in the sediment.

3. SCATTERING

3.1 OVERVIEW

Acoustic backscatter from sediments can be divided into two groups; surface scattering of the incident wave and volume scattering of a refracted or evanescent wave inside the sediment. The latter of these types will be the subject of the following discussion. The emphasis will be on the case where the wavefront is at a subcritical grazing angle.

Measurements of acoustic backscatter from sediments at shallow grazing angles began in the 1950s with a measurement by Urick.[14] From 1964 to the early 1980s the one outstanding source of data was that of McKinney and Anderson.[15] Since 1982 the amount of data available has doubled, with work being done in the USA, the UK, the USSR, and Canada. The following is a statistical study of these data. The trends suggest that gas bubbles may be a dominant factor in the backscattering strength of sediments. This hypothesis will be explored with a simple model.

3.2 STATISTICAL STUDY

Figure 3.1 is a scatter plot incorporating all of the above data. In this plot the measured backscattering strength is plotted against grain diameter in wavelengths. The data span a region between a theoretical upper limit associated with Lambert's rule and a lower limit defined by the results of some experiments by Nolle[16] with carefully graded laboratory sands.

When each of the above data sites is examined separately, two kinds of trends are apparent. In Fig. 3.2 data points from the same site are connected with lines. In the first group of data points the backscattering strength increases steadily with grain size just as it does in Nolle's data. The second group of data points exhibits a broad maximum in the backscatter intensity when the grain diameter is about $10^{-2.5}$ wavelengths. The fact that this coincides with the

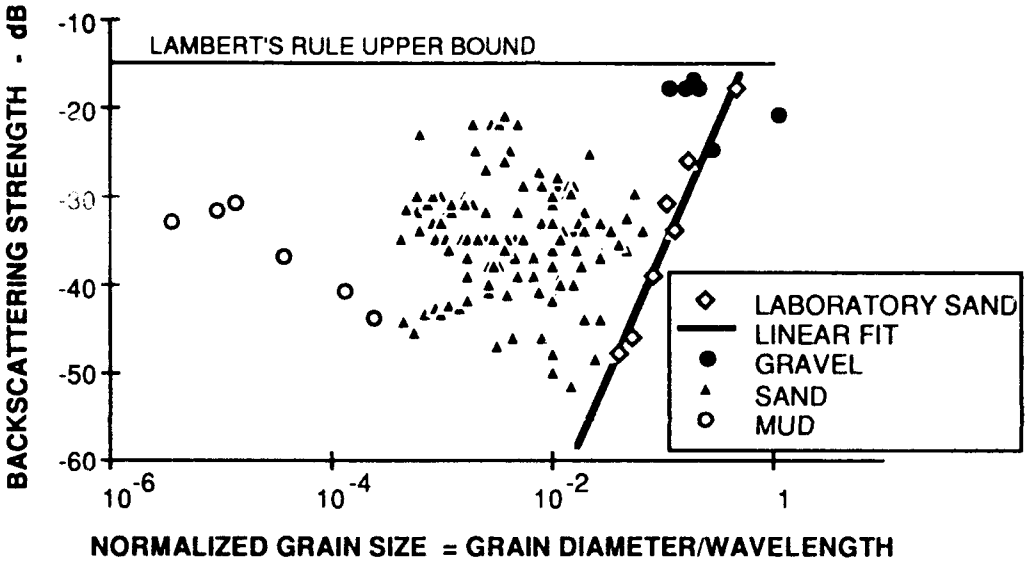

FIGURE 3.1
EXPERIMENTAL MEASUREMENTS OF BOTTOM BACKSCATTERING STRENGTH AS A FUNCTION OF GRAIN SIZE AT A GRAZING ANGLE OF 10° FROM ALL PUBLISHED SOURCES

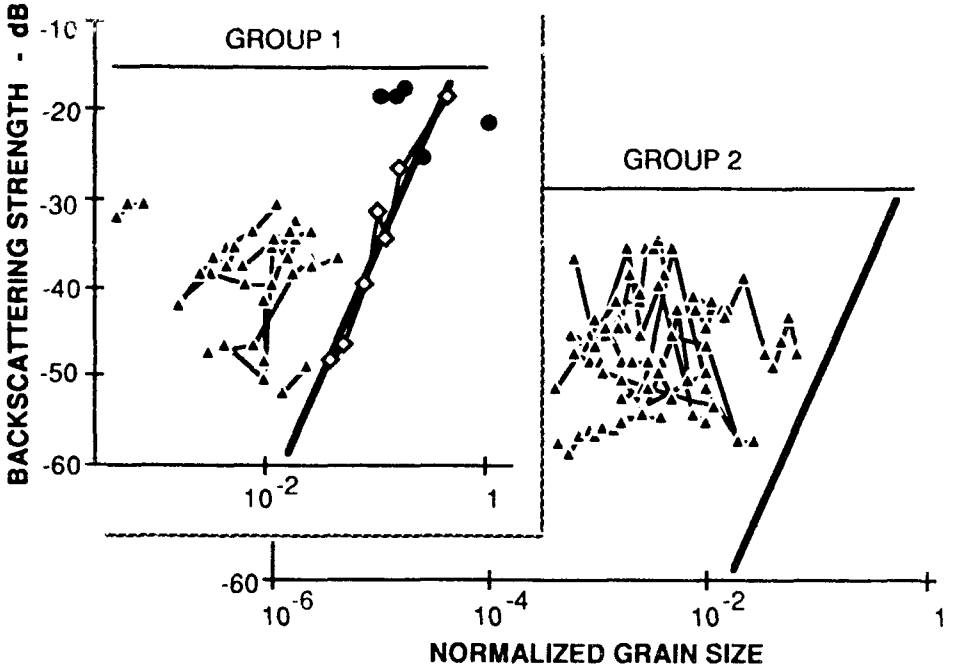

FIGURE 3.2
EXPERIMENTAL MEASUREMENTS OF BOTTOM BACKSCATTERING STRENGTH AS A FUNCTION OF GRAIN SIZE AT A GRAZING ANGLE OF 10°
GROUPS 1 AND 2

resonance diameter of gas bubbles suggests that this set of data may be influenced by gas content in the sediment.

3.3 PRELIMINARY MODEL

A preliminary model for scattering from trapped gas bubbles begins with the following assumptions: (1) the bubbles interact with the evanescent wave, which is known to penetrate approximately one wavelength into a medium; (2) the bubble size distribution follows the same form as the pore size distribution; and (3) the bubbles exist in the fluid component of the saturated sediment and have a scattering cross section approximately the same as bubbles in open water.

The motivation behind assumption (1) above is that an incident grazing angle of 10° is subcritcal for refraction via the Biot fast wave. A relaxation of this assumption to include Biot slow wave penetration will be studied in future work.

3.3.1 Bubble Size Distribution

The bubble size distribution is estimated in the following manner. Consider the grains of approximately the same radius r_g, approximately round, and close packed, as in Fig. 3.3. The radius of a sphere that can just fit into the pore space is r_v. Let us define

$$y_{gr} = \ln\left(\frac{r_g}{r_v}\right) \quad . \tag{3.1}$$

Let us also define a volume ratio,

$$R_{vd} = \frac{\text{Pore volume}}{\text{Grain volume}} \cong \frac{(8r_g^3 - \frac{4}{3}\pi r_g^3)}{\frac{4}{3}\pi r_g^3} = \frac{6-\pi}{\pi} \quad . \tag{3.2}$$

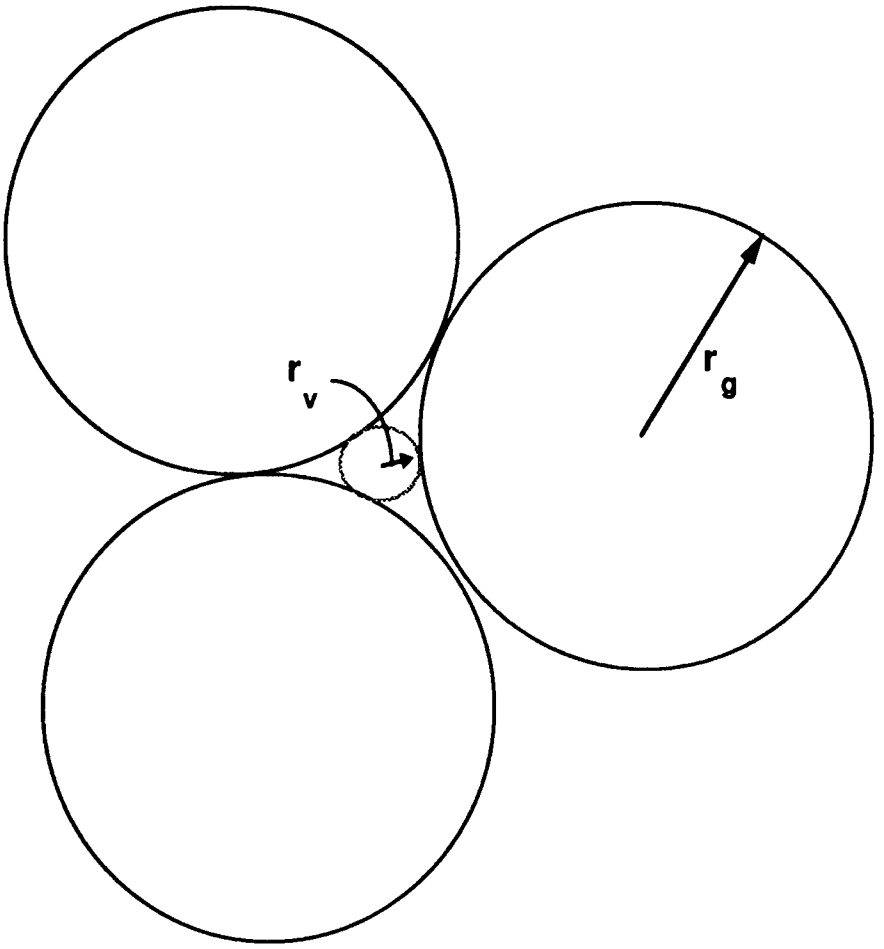

FIGURE 3.3
CLOSE PACKED SEDIMENT GRAINS

ARL:UT
AS-92-166
FAB - DS
7 - 1 - 92

The grains are part of a population. Let $y=\ln(r_g)$ and let f(y) be the density function of the grain population in (kg/m^3)/neper. The volume of the void between grains of sizes between y and $y+y_{gr}$ is given by

$$V_v(y) = \frac{1}{\rho}\int_y^{y+y_{gr}} f(s)\ R_{vd}\ ds \quad (m^3_{void}/m^3_{total\ space}) \quad , \qquad (3.3)$$

where ρ is the density of the grain material and s is a dummy variable of integration. The total volume of grains smaller than y is

$$V_g(y) = \frac{1}{\rho}\int_{-\infty}^{y} f(s)\ ds \qquad (m^3_{grains}/m^3_{total\ space}) \quad . \qquad (3.4)$$

The volume of empty void space between the grains of the stated size range is then

$$V_e(y) = \begin{cases} V_v(y) - V_g(y) & \text{if } V_v(y) > V_g(y) \\ 0 & \text{if } V_v(y) \le V_g(y) \end{cases} \quad . \qquad (3.5)$$

The second of these two possibilities represents a case where there are so many small grains and so few large grains that the large grains are no longer closely packed. It is advantageous to define a void distribution function $f_e(y)$ as follows:

$$\int_y^{y+y_{gr}} f_e(s)\ ds = V_e(y) \quad . \qquad (3.6)$$

In explicit form, then, f_e is given by

$$f_e(y) = \left[\frac{dV_e(s)}{ds}\right]_{s=y+y_{gr}} - \left[\frac{dV_e(s)}{ds}\right]_{s=y}$$

$$= \frac{1}{\rho}\left[R_{vd}f(y+2y_{gr})-(R_{vd}+1)f(y+y_{gr})+f(-\infty)\right]$$

$$- \frac{1}{\rho}\left[R_{vd}f(y+y_{gr})-(R_{vd}+1)f(y)+f(-\infty)\right]$$

$$= \frac{1}{\rho}\left[R_{vd}\ f(y+2\ y_{gr}) - (1+2\ R_{vd})\ f(y+y_{gr}) + (R_{vd}+1)\ f(y)\right] . \quad (3.7)$$

Let the grain density function f(y) be a normal distribution:

$$f(y) = \gamma \frac{\exp\left(-\frac{(y-y_0)^2}{2\sigma_y^2}\right)}{\sqrt{2\pi\sigma_y^2}} , \quad (3.8)$$

where γ is a proportionality constant equal to ρ(1-porosity), y_0 is the mean, and σ_y is the standard deviation. Upon substituting this into Eq. (3.7),

$$f_e(y) = \frac{\gamma}{\rho}\left\{ R_{vd} \frac{\exp\left(-\frac{(y+2y_{gr}-y_0)^2}{2\sigma_y^2}\right)}{\sqrt{2\pi\sigma_y^2}}\right.$$

$$\left. - (1+2R_{vd}) \frac{\exp\left(-\frac{(y+y_{gr}-y_0)^2}{2\sigma_y^2}\right)}{\sqrt{2\pi\sigma_y^2}} + (R_{vd}+1) \frac{\exp\left(-\frac{(y-y_0)^2}{2\sigma_y^2}\right)}{\sqrt{2\pi\sigma_y^2}}\right\} . \quad (3.9)$$

Equation (3.9) is an equation for the total volume of empty space between grains of diameter $r_g=e^y$ in $(m^3_{void}/m^3_{total\ space})$/neper. The gas volume fraction is assumed to be this quantity multiplied by a constant less than or equal to one:

$$f_b(y) = \xi\ f_e(y). \quad (3.10)$$

The case where $\xi = 1$ corresponds to a dry sediment, i.e., 100% saturated with gas. In general ξ is taken to be a constant less than one. Equation (3.10) thus is an expression for the gas density function in $(m^3_{gas}/m^3_{total\ space})$/neper.

The bubbles in the pores are allowed to have radii smaller than r_v. This might be the case for nonspherical grains which may pack closer than spherical ones. It is also possible that a bubble will not occupy the maximum possible amount of pore space. We introduce a constant, y_b, that relates the bubble radius to the pore radius.

$$y_b = \ln\left(\frac{r_b}{r_v}\right) \quad .$$

To get a bubble size distribution function (number of bubbles/$m^3_{total\ space}$)/neper, divide Eq. (3.10) by the bubble volume:

$$f_{bn}(y) = \frac{f_b(y)}{\left(\frac{4}{3}\pi r_v^3\right)} = \frac{f_b(y)}{\left(\frac{4}{3}\pi e^{3(y-y_{gr}+y_b)}\right)} \quad .$$

Upon combining Eqs. (3.9), (3.10), and (3.12), the bubble distribution is expressible in the following form:

$$f_{bn}(y) = \frac{3\xi\gamma}{4\pi\rho e^{3(y-y_{gr}+y_b)}} \left\{ R_{vd} \frac{\exp\left(-\frac{(y+2y_{gr}-y_0)^2}{2\sigma_y^2}\right)}{\sqrt{2\pi\sigma_y^2}} \right.$$

$$\left. - (1 + 2R_{vd}) \frac{\exp\left(-\frac{(y+y_{gr}-y_0)^2}{\sqrt{2\sigma_y^2}}\right)}{\sqrt{2\pi\sigma_y^2}} + (R_{vd}+1) \frac{\exp\left(-\frac{(y-y_0)^2}{2\sigma_y^2}\right)}{\sqrt{2\pi\sigma_y^2}} \right\}. \qquad (3.13)$$

3.3.2 Scattering Integral

We begin with the scattering cross-section for a single bubble of radius r_b insonified by a signal of frequency f. This is assumed equal to the in-water scattering cross-section given by Medwin[17] and Wildt[18]

$$\sigma(r_b) = \frac{4\pi r_b^2}{\left[(f_r / f)^2 - 1\right]^2 + \delta^2} \quad , \tag{3.14}$$

where rf_r is approximately 3 and d is approximately 0.1. The total backscattering cross-section per unit area for a collection of bubbles of size distribution $f_{bn}(y)$ is given by

$$\sigma_b = \int h\, \sigma(r_b)\, f_{bn}(y)\, dy \quad , \tag{3.15}$$

where h is the depth of penetration of the evanescent wave, taken to be one wavelength. The backscattering strength is then given by

$$S_b = 10 \log \left(\frac{\sigma_b}{4\pi}\right) \quad . \tag{3.16}$$

The parameters that influence the backscattering strength are: (1) the gas fraction, (2) the sediment sound speed, which determines the layer thickness, (3) the mean, (4) the standard deviation of the logarithm of the sediment grain size, and (5) bubble radius/pore radius ratio. Only the gas fraction is completely unknown. In the following analysis this is considered a free parameter and varied to fit the data.

3.3.3 Comparison with Experiment

Figure 3.4 contains the data from four experimental sites, plotted separately. Overlaid onto these plots are curves that represent the theoretical backscattering strength from Eq. (3.16) above. In each case the gas fraction and bubble radius/pore radius ratio was varied to achieve a best fit. The

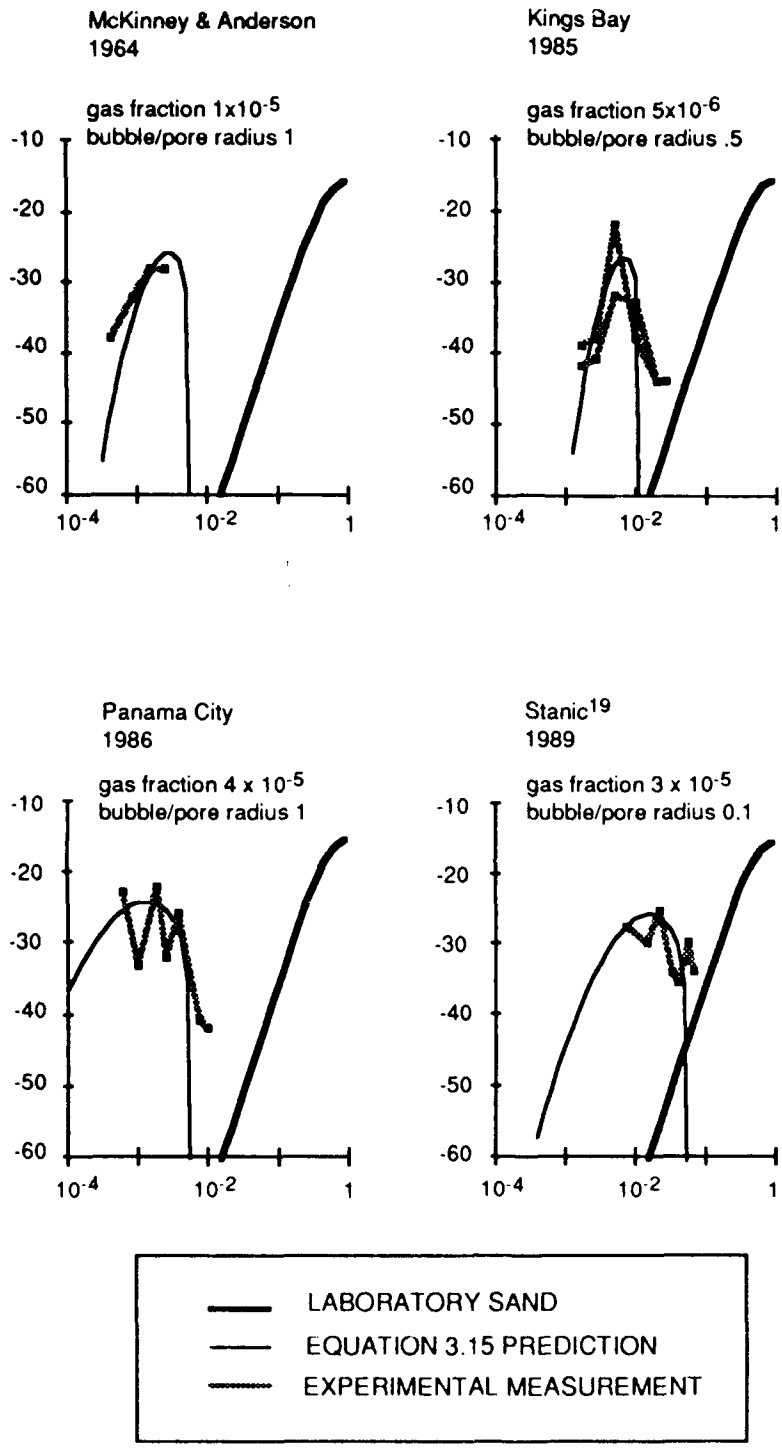

FIGURE 3.4
A COMPARISON OF EXPERIMENTAL DATA WITH BACKSCATTERING STRENGTHS PREDICTED BY EQ. (3.15)

ARL:UT
AS-92-167
FAB - DS
7 - 1 - 92

appropriate gas fractions ranged from $5x10^{-6}$ to $4x10^{-5}$. The bubble radius/pore radius ratios were between 0.1 and 1.

This work is a preliminary study. Several issues need to be addressed in order to obtain a reliable model. They include: (1) the actual scattering cross-section of bubbles entrapped in sediment, (2) the mechanism of acoustic coupling, (3) further work on the bubble population density function and its causes, (4) experimental measurement of bubble population density, and (5) the collection of more experimental data to more conclusively demonstrate the effect of gas content on backscattering strength.

This page intentionally left blank.

4. CONCLUSION

The acoustic penetration modeling based on the Biot theory differs significantly from that based on viscoelastic theory. Specifically, the Biot theory predicts much more acoustic penetration at shallow grazing angles than does viscoelastic theory. Bottom reflection coefficients are also noticeably influenced. The backscatter problem will likely be influenced, especially at shallow grazing angles.

Experimental results suggest that gas content may contribute significantly to the observed backscattering strength in some sediments. Very low gas fractions can generally account for the observed behavior. These gas fractions are so small that they will be very difficult to measure. Furthermore, the observed frequency dependence is consistent with the resonance behavior of gas bubbles.

This page intentionally left blank.

APPENDIX

A COMPARISON OF THE BIOT EQUATIONS AS GIVEN BY STERN TO THOSE ORIGINALLY PUBLISHED BY BIOT

This page intentionally left blank.

Our work originates with a computer model developed by Stern which incorporates the Biot theory. There are some differences between Stern's version of the Biot equations and those originally published by Biot. Those differences can be traced to differences in notation. The following is a comparison of the Stern's and Biot's equations. It begins with the Biot equations and applies the differences in notation to arrive at the equations Stern uses.

Start with the Biot equations given in Biot, 1956:

$$N\nabla^2\mathbf{u} + \text{grad}[(A+N)e + Q\varepsilon] = \frac{\partial^2}{\partial t^2}(\rho_{11}\mathbf{u} + \rho_{12}\mathbf{U}) + b\frac{\partial}{\partial t}(\mathbf{u} - \mathbf{U})$$

$$\text{grad}[Qe + R\varepsilon] = \frac{\partial^2}{\partial t^2}(\rho_{12}\mathbf{u} + \rho_{22}\mathbf{U}) - b\frac{\partial}{\partial t}(\mathbf{u} - \mathbf{U}) \quad ,$$

u = solid displacement vector
U = fluid displacement vector
e = div**u**
ε = div**U**
N,A,Q,R,b = constants
ρ_{11},ρ_{12},ρ_{22} = constants involving the densities of the fluid and solid components:
$\rho_{11}+\rho_{12}=\rho_1=(1-\beta)\rho_s$= mass of solid/unit volume of aggregate
$\rho_{12}+\rho_{22}=\rho_2=\beta\rho_f$= mass of fluid/unit volume of aggregate
$\rho_{11}+2\rho_{12}+\rho_{22}=\rho$=mass density of saturated sediment
ρ_{12}= coupling coefficient
β=porosity

Stern uses the following parameters in his notation:

$$\mathbf{w}=b(\mathbf{u}-\mathbf{U}), \text{ and}$$
$$z=\mathrm{div}\mathbf{w}.$$

Make the following substitutions to get to the notation of Stern:

$$\mathbf{U}=\mathbf{u}-\mathbf{w}/b, \text{ and}$$
$$e = e-z/b.$$

We now have:

$$N\nabla^2\mathbf{u} + \nabla[(A+N)e + Q(e-\frac{\zeta}{\beta})] = \frac{\partial^2}{\partial t^2}(\rho_{11}\mathbf{u} + \rho_{12}(\mathbf{u}-\frac{\mathbf{w}}{\beta})) + b\frac{\partial}{\partial t}(\mathbf{u} - \mathbf{u}+\frac{\mathbf{w}}{\beta}) \text{ , and}$$

$$\nabla[Qe + Re - \frac{R}{\beta}\zeta] = \frac{\partial^2}{\partial t^2}(\rho_{12}\mathbf{u} + \rho_{22}(\mathbf{u} - \frac{\mathbf{w}}{\beta})) - b\frac{\partial}{\partial t}(\mathbf{u} - \mathbf{u}+\frac{\mathbf{w}}{\beta}).$$

Upon carrying the del operator through the constants and making further simplifications, we have:

$$N\nabla^2\mathbf{u} + (A+N+Q)\nabla e - \frac{Q}{\beta}\nabla\zeta = (\rho_{11}+\rho_{12})\ddot{\mathbf{u}} - \frac{\rho_{12}}{\beta}\ddot{\mathbf{w}} + \frac{b}{\beta}\dot{\mathbf{w}} \text{ , and} \qquad (A.1)$$

$$(Q + R)\nabla e - \frac{R}{\beta}\nabla\zeta = (\rho_{12} + \rho_{22})\ddot{\mathbf{u}} - \frac{\rho_{22}}{\beta}\ddot{\mathbf{w}} - \frac{b}{\beta}\dot{\mathbf{w}} . \qquad (A.2)$$

Add Eqs. (A.1) and (A.2):

$$N\nabla^2\mathbf{u} + (A+N+2Q+R)\nabla e - \frac{(Q+R)}{\beta}\nabla\zeta = (\rho_{11}+2\rho_{12}+\rho_{22})\ddot{\mathbf{u}} - \frac{(\rho_{12}+\rho_{22})}{\beta}\ddot{\mathbf{w}} \text{ , (A.3)}$$

divide Eq. (A.2) by b:

$$\frac{(Q + R)}{\beta}\nabla e - \frac{R}{\beta^2}\nabla\zeta = \frac{(\rho_{12} + \rho_{22})}{\beta}\ddot{\mathbf{u}} - \frac{\rho_{22}}{\beta^2}\ddot{\mathbf{w}} - \frac{b}{\beta^2}\dot{\mathbf{w}} , \qquad (A.4)$$

make the following substitutions in Eqs. (A.3) and (A.4):

$N=m$

$A+N+2Q+R=H-2m$

$(Q+R)/b=C$

$r_{11}+2r_{12}+r_{22}=r$

$r_{12}+r_{22}=br_f$

$R/b^2=M$

$r_{22}/b=cr_f$

$b/b^2=Fh/k.$

We now have:

$$\mu\nabla^2\mathbf{u} + (H-2\mu)\nabla e - C\nabla\zeta = \rho\ddot{\mathbf{u}} - \rho_f\ddot{\mathbf{w}}$$

$$C\nabla e - M\nabla\zeta = \rho_f\ddot{\mathbf{u}} - \frac{c\rho_f}{\beta}\ddot{\mathbf{w}} - \frac{F\eta}{\kappa}\dot{\mathbf{w}} \quad .$$

The above equations are Eqs. (12) and (13) in Stern, 1985.

This page intentionally left blank.

REFERENCES

1. N. P. Chotiros, "High Frequency Acoustic Penetration Analysis," Applied Research Laboratories Technical Report No. 89-28 (ARL-TR-89-28), Applied Research Laboratories, The University of Texas at Austin, May 1989.

2. N. P. Chotiros and M. L. Ramaker, "High Frequency Acoustic Penetration of Sandy Ocean Sediments," Presentation at 121st Meeting of the Acoustical Society of America, J. Acoust. Soc. Am. 89(4), Pt. 2, 1908 (1991).

3. F. A. Boyle and N. P. Chotiros, "Experimental Detection of a Slow Acoustic Wave in Sediment at Shallow Grazing Angles," Applied Research Laboratories Technical Report No. 91-14 (ARL-TR-91-14), Applied Research Laboratories, The University of Texas at Austin, May 1991.

4. N. P. Chotiros and F. A. Boyle, "Gas Bubbles in Ocean Sediments and High-Frequency Acoustic Backscattering Strength," Presentation at 121st Meeting of the Acoustical Society of America, J. Acoust. Soc. Am. 89(4), Pt. 2, 1852 (1991).

5. M. A. Biot, "Theory of Propagation of Elastic Waves in a Fluid-Saturated Porous Solid, I. Low-Frequency Range," J. Acoust. Soc. Am. 28, 168-178 (1956).

6. M. A. Biot, "Theory of Propagation of Elastic Waves in a Fluid-Saturated Porous Solid, II. Higher Frequency Range," J. Acoust. Soc. Am. 28, 179-191 (1956).

7. M. Stern, A. Bedford, and H. R. Millwater, "Wave Reflection from a Sediment Layer with Depth-Dependent Properties," J. Acoust. Soc. Am. 77, 1781-1788 (1985).

8. N. P. Chotiros, "High Frequency Bottom Penetration: Panama City Experiment Analysis III," Applied Research Laboratories Technical Report No. 91-18 (ARL-TR-91-18), Applied Research Laboratories, The University of Texas at Austin, July 1991.

9. N. P. Chotiros, "High Frequency Acoustic Penetration Analysis," Applied Research Laboratories Technical Report No. 89-28 (ARL-TR-89-28), Applied Research Laboratories, The University of Texas at Austin, May 1989.

10. F. A. Boyle and N. P. Chotiros, "Experimental Detection of a Slow Acoustic Wave in Sediment at Shallow Grazing Angles," Applied Research Laboratories Technical Report No. 91-14 (ARL-TR-91-14), Applied Research Laboratories, The University of Texas at Austin, May 1991.

11. J. A. Hawkins, Jr., and A. Bedford, "A Variational Model for Bubbly Liquids: Reflection from a Liquid-Bubbly Interface," Presentation at 120th Meeting of the Acoustical Society of America, J. Acoust. Soc. Am. 88(1) S131 (1990).

12. M. Stern, A. Bedford, and H. R. Millwater, "Wave Reflection from a Sediment Layer with Depth-Dependent Properties," J. Acoust. Soc. Am. 77, 1781-1788 (1985).

13. J. L. Darrouzet, J. C. Molis, and N. P.Chotiros, "Grain Bulk Modulus of Sand," Presentation at 122nd Meeting of the Acoustical Society of America, J. Acoust. Soc. Am. 90(4), Pt. 2, 2370 (1991).

14. R. J. Urick, "Backscattering of Sound from a Harbor Bottom," J. Acoust. Soc. Am. 26(2), 231-235 (1954).

15. C. M. McKinney and C. D. Anderson, "Measurements of Backscattering of Sound from the Ocean Bottom," J. Acoust. Soc. Am. 36(1), 158-163 (1964).

16. A. W. Nolle, J. F. Mifsud, W. R. Runyan, and M. B. Ward, "Acoustical Properties of Water-Filled Sands," J. Acoust. Soc. Am. 35, 1394-1408 (1963).

17. H. Medwin, "Acoustical Determinations of Bubble Size Spectra," J. Acoust. Soc. Am. 62(4), 1041-1044 (1977).

18. R. Wildt, ed., "Acoustic Theory of Bubbles," in *Physics of Sound in the Sea*, NDRC Summary Technical Report, Div. 6, Vol. 8, Chap. 28, Washington, D.C. (1946).

19. S. Stanic, K. B. Briggs, P. Fleischer, W. B. Sawyer, and R. I. Ray, "High Frequency Experiments, Part II: Environmental Characterization Data," NORDA Technical Note 376, Naval Ocean Research and Development Activity, Stennis Space Center, Mississippi, May 1989.

This page intentionally left blank.

19 June 1992

DISTRIBUTION LIST FOR
ARL-TR-92-12
Final Report Under Contract N00039-91-C-0082,
TD No. 01A1006, Bottom Penetration at Shallow Grazing Angles II

Copy No.

Commanding Officer
Naval Research Laboratory
Stennis Space Center, MS 39529-5004

1	Attn:	R. Farwell (Code 240)
2		D. Young (Code 333)
3		P. Fleischer (Code 361)
4		K. Briggs (Code 333)
5		P. Valent (Code 310)
6		R. Love (Code 243)
7		B. Adams (Code 113)
8		E. Franchi (Code 200)
9		S. Stanic (Code 243)
10 - 21		Library (Code 125L)

Office of the Chief of Naval Research
Office of Naval Technology
Department of the Navy
Arlington, VA 22217-5000

22	Attn:	R. Obrochta (Code 1125OA)
23		J. Kravitz (Code 1125GG)
24		M. Orr (Code 11250A)
25		K. Lackie (Code 125)
26		D. Houser (Code 232)
27		A. Faulstich (Code 23)
28		W. Ching (Code 235)
29		T. Goldsberry (Code 231)

Commanding Officer
Naval Oceanographic Office
Stennis Space Center, MS 39522-5001

30	Attn:	W. Jobst (Code OA)
31		J. Bunce (Code OW)
32		R. Christensen (Code OAR)
33		E. Beeson (Code OARR)

Distribution List for ARL-TR-92-12 under Contract N00039-91-C-0082,
TD No. 01A1006
(cont'd)

Copy No.		
		Office of Naval Research Detachment Stennis Space Center, MS 39529-5004
34	Attn:	B. Blumenthal (ONR DET 125)
35		E. Chaika (ONR DET 125)
		Commander Naval Oceanography Command Stennis Space Center, MS 39522-5000
36	Attn:	D. Durham (Code N5A)
		Commander Naval Sea Systems Command Department of the Navy Washington, D.C. 20362-5101
37	Attn:	J. Grembi (PMS407B)
38		D. Gaarde (PMS407D4)
39		J. Neely (PMS418W)
40		T. Douglass (PMS402B)
41		H. Grunin (PMS402)
42		A. Knobler (PMS406B)
		Commander Dahlgren Division Naval Surface Warfare Center Dahlgren, VA 22448-5000
43	Attn:	S. Burgess (NGM Library)
		Commander Dahlgren Division Naval Surface Warfare Center Silver Spring, MD 20903-5000
44	Attn:	S. Martin (Code U24)
45		J. Sherman (Code U20)
46		M. Stripling (Code U04)
		Commanding Officer Coastal Systems Station Dahlgren Division Naval Surface Warfare Center Panama City, FL 32407-5000
47	Attn:	R. Johnson (Code 210T)
48		D. Todoroff (Code 2120)

Distribution List for ARL-TR-92-12 under Contract N00039-91-C-0082,
TD No. 01A1006
(cont'd)

Copy No.		
		Officer in Charge Naval Undersea Warfare Center Division New London, CT 06320-5594
49	Attn:	W. Roderick (Code 33A3)
50		J. Geary (Code 3221)
51		W. Cary (Code 33A)
52		J. Chester (Code 3331)
53		P. Koenig (Code 3331)
		Commanding Officer Naval Undersea Warfare Center Division Newport, RI 02841-5047
54	Attn:	J. Kelly (Code 3632)
55		F. Aidala (Code 362)
56		W. Gozdz (Code 36291)
		Commanding Officer Naval Command, Control and Ocean Surveillance Center RDT&E Center San Diego, CA 92152-5000
57	Attn:	R. Anderson (Code 54)
		Office of the Chief of Naval Operations Department of the Navy Washington, D.C. 20360
58	Attn:	R. Widmayer (OP 374T)
59		R. Winokur (OP 096T)
60		K. Martello (OP 954F1)
61		T. Fraim (OP 986G)
62		R. James (OP 006DX)
63		H. Montgomery (OP 9878)
64		J. Boosman (OP 987J)
		Commander Mine Warfare Command Charleston Naval Base Charleston, SC 29408
65	Attn:	G. Pollitt (Code N4A)
66		B. O'Connel (Code N3A)

Distribution List for ARL-TR-92-12 under Contract N00039-91-C-0082,
TD No. 01A1006
(cont'd)

Copy No.

67 - 78	Commanding Officer and Director Defense Technical Information Center Cameron Station, Building 5 5010 Duke Street Alexandria, VA 22314
	Applied Physics Laboratory The University of Washington 1013 NE 40th Street Seattle, WA 98105
79	Attn: D. Jackson
80	Library
	Applied Research Laboratory The Pennsylvania State University P. O. Box 30 State College, PA 16804
81	Attn: S. McDaniel
82	D. McCammon
83	F. Symons
84	J. Beebe
85	D. Upshaw
86	E. Liszka
87	Library
	Presearch, Inc. 8500 Executive Park Avenue Fairfax, VA 22031
88 - 90	Attn: J. R. Blouin
	Physics Department The University of Texas at Austin Austin, TX 78712
91	Attn: W. D. McCormick
92	M. Fink
93	T. Griffy
	Aerospace Engineering Department The University of Texas at Austin Austin, TX 78712
94	Attn: M. Bedford
95	Robert A. Altenburg, ARL:UT

Distribution List for ARL-TR-92-12 under Contract N00039-91-C-0082,
TD No. 01A1006
(cont'd)

Copy No.	
96	Hollis Boehme, ARL:UT
97	Frank A. Boyle, ARL:UT
98	Nicholas P. Chotiros, ARL:UT
99	John M. Huckabay, ARL:UT
100	T. G. Muir, ARL:UT
101 - 107	Library, ARL:UT
108 - 113	Reserve, ARL:UT